CONTRIBUTIONS OF MASS CHANGES OVER GLOBAL MOUNTAIN GLACIERS AND ICE SHEETS TO SEA LEVEL RISE FROM 2002 TO 2022

Wei Wang[1], Yunzhong Shen*[2], Qiujie Chen[3]
[1]PhD Candidate, College of Surveying and Geo-Informatics, Tongji University,
Shanghai 200092, P. R. China.
Email: wangwei_96@tongji.edu.cn

[2]Professor, College of Surveying and Geo-Informatics, Tongji University,
Shanghai 200092, P. R. China.
Email: yzshen@tongji.edu.cn

[3]Professor, College of Surveying and Geo-Informatics, Tongji University,
Shanghai 200092, P. R. China.
Email: qiujiechen@tongji.edu.cn

KEY WORDS: Mountain Glaciers; Ice Sheets; Sea Level Rise; Climate Change; Satellite Gravimetry

ABSTRACT: The Greenland Ice Sheet (GrIS), Antarctic Ice Sheet (AIS), and global Mountain Glaciers (MGs) are highly susceptible to climate change and exert a significant influence on the global mean sea level (GMSL). To extend the global ice mass change record and qualify corresponding contributions to GMSL, we conducted a comprehensive investigation into the mass changes in global ice-covered regions from April 2002 to December 2022, using newly released satellite gravimetry data. Our study reveals a pronounced decline in global ice mass during this period, accompanied by large interannual fluctuations. Overall, the total ice mass loss amounts to 13,951 Gt/yr, corresponding to a GMSL rise of 1.6 ± 0.1 mm/yr. Specifically, global MGs, the GrIS, and AIS contribute mass changes at −224.90±32.02 Gt/yr, –266.80±7.37 Gt/yr, and –143.64±8.86 Gt/yr, respectively. Notably, among the 17 MGs, the Alaska glacier demonstrates the most substantial loss trend at −72.38±4.76 Gt/yr, accounting for approximately one-third of the total MGs, followed by the Arctic Canada North, Arctic Canada South, Southern Andes and High Mountain Asia glaciers, with a mass loss trend of −36.05±0.99, −27.19±1.39, −24.27±5.54 and −23.00±4.60 Gt/yr. Analyzing biennial mass changes, we observe significant interannual mass variations for individual glaciers closely associated with atmospheric circulation anomalies. Among the 11 climate indices, the North Pacific Gyre Oscillation (NPGO), Pacific Decadal Oscillation (PDO), and Multivariate ENSO Index (MEI) stand out as the most crucial climate indices for predicting ice mass and sea level fluctuations.

1. INTRODUCTION

Polar ice sheets and global mountain glaciers are highly sensitive to climate change and constitute the primary contributors to global sea level rise. If the Antarctic Ice Sheet (AIS), Greenland Ice Sheet (GrIS), and mountain glaciers were to melt completely, they could individually lead to a sea level rise of approximately 58 meters (Lythe et al., 2001), 7 meters (Morlighem et al., 2017), and 0.32 meters (Farinotti et al., 2019). Therefore, quantitatively assessing the mass changes of global ice sheets and glaciers holds paramount importance in predicting sea level changes and comprehending global climate change.

Geodetic and glaciological methods observe changes in glacier volume and mass. In-situ measurements can date back to the 1960s and consist mostly of front positions, snow depths of winter accumulation, and ablation at ice-stake locations (WGMS, 2021). Due to the substantial resources required for glacier surveys, there is significant variability in observation coverage across different regions. On a global scale, less than 100 glaciers have been continuously monitored, with approximately 200,000 glaciers globally (WGMS, 2021). Consequently, in-situ measurements are delicate to estimate large-scale glacier changes (Gardner et al., 2013). The numerical model simulates the regional mass change resulting from the surface mass budget. Ice discharge due to the calving of icebergs from glaciers that terminate in the sea, denoted D, is added to the surface mass-budget model results to account for the total regional ice loss. However, there are too few records of glacier mass budget and near-surface temperature for some glaciers to calibrate the model (Gardner et al., 2011).

Since the era of satellite technology, various satellite observational data have been utilized to estimate the mass changes of glaciers. Satellite laser altimetry of the ICESat (Ice, Cloud, and Land Elevation Satellite), ICESat-2 (Zwally et al., 2002), and radar altimetry of CryoSat-2 (Jacob et al., 2023) measure the change in land-ice volume. Optical stereo-photogrammetry (e.g., ASTER, Advanced Spaceborne Thermal Emission, and Reflection Radiometer) provides the Digital Elevation Model of land ice (Hugonnet et al., 2021). Nonetheless, these methods struggle to accurately estimate the total mass loss from glaciers melting worldwide due to incomplete spatial coverage and a poorly known density (Jacob

et al., 2023). Satellite gravimetry, mainly the GRACE mission, can directly infer surface mass changes with monthly temporal resolution and spatial resolution of several hundred kilometers using the KBRR (K-Band Ranging Ranging) technique after glacial isostatic adjustment (GIA) and the Little Ice Age (LIA) correction. Previous studies have used GRACE data to estimate the mass changes of specific glaciers for the periods covered by the GRACE mission, such as Alaska (Doumbia et al., 2020; Arendt et al., 2013), High Mountain Asia (Xiang et al., 2021), the Russian Arctic (Ciracì et al., 2018), and the Canadian Arctic (Gardner et al., 2011; Gardner et al., 2012). With all global glaciers considered, Jacob et al. (2012) found a mass loss trend of –148±30 Gt/yr between 2003 and 2010 with GRACE RL05 data, and the result estimated with GRACE RL06 data is –199 ± 32 Gt/yr between 2002 and 2016 (Wouters et al., 2019). With the launch of the GRACE-FO satellite, Ciracì et al. (2020) validated the continuity of glacier mass change estimation using GRACE-FO data and estimated the global mountain glacier mass change trend for 2002–2019.

In light of the drastic changes in the global climate system and the prolonged record of GRACE-FO data, accompanied by enhancements in the spatial resolution of GRACE/GRACE-FO estimates (Save et al., 2016; Save, 2020), it has become imperative to reevaluate the mass changes of global mountain glaciers and polar ice sheets. Therefore, this study aims to quantitatively estimate the contributions of each glacier and ice sheet to fluctuations in the global mean sea level, conduct an analysis of their temporal characteristics, and delve into the underlying mechanisms driving changes in glacier mass. The rest of the paper is organized as follows: The adopted data and method are described in Section 2. Section 3 demonstrates the mass changes of ice sheets and global mountain glaciers, their comparison with other mass change estimates, and links to atmospheric circulation. Finally, conclusions are presented in Section 4.

2. DATA AND METHODS

2.1 Study area

The study area consists of the land-ice-covered regions of polar ice sheets, i.e., the Greenland Ice Sheet (GrIS) and the Antarctic Ice Sheet (AIS), as well as the global mountain glaciers and ice gaps. Here we used the global mountain glacier definition provided by the Consortium Randolph Glacier Inventory (RGI) as shown in Figure 1; region names are as follows, 1: Alaska(ALA), 2: Western Canada and US(WCU), 3: Arctic Canada North(ACN), 4: Arctic Canada South(ACS), 5: Greenland Ice Sheet (GrIS); 6: Iceland(ICE), 7: Svalbard(SJM), 8: Scandinavia(SCA), 9: Russian Arctic(RA), 10: North Asia(NA), 11: Central Europe(CE), 12: Caucasus and Middle East(CME), 13–15: High Mountain Asia (HMA), 16: Low Latitudes(LL), 17: Southern Andes(SA), 18: New Zealand(NZ), 19: Antarctic Ice Sheet (AIS). Since the spatial resolution of GRACE/GRACE-FO observations is approximately 300 km and the separation of the ice sheet mass change signal and their peripheral ice caps and glaciers is challenging, the mass changes of RGI5 (peripheral ice caps and glaciers of the GrIS) and RGI19 (peripheral ice caps and glaciers of the GrIS) are not separated from the corresponding ice sheet. As a result, we divided global land ice into 17 mountain glaciers and two ice sheets, i.e., the GrIS and AIS.

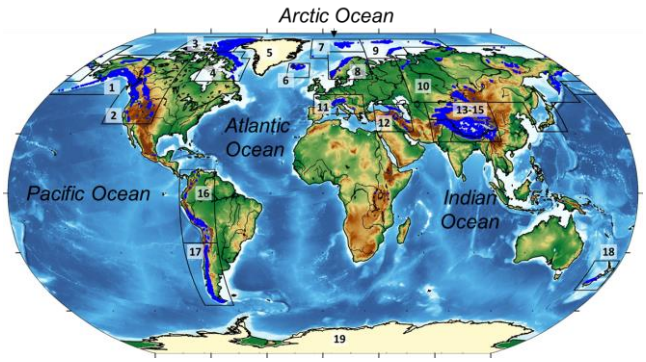

Figure 1. Outlines of the RGI 6.0 regions. Locations of the mountain glaciers and ice sheets are shown in blue and light yellow, respectively. The GrIS and AIS contain their peripheral ice caps and glaciers in this study.

2.2 Ice mass changes from GRACE/GRACE-FO Data

The GRACE/GRACE-FO mascon solutions (RL06, version 02) provided by the Centre for Space Research (CSR) at the University of Texas Austin (Save, 2020; Save et al., 2016) are used in this study. The period is from April 2002 to December 2022, and the gap between the GRACE and GRACE-FO missions is filled using the extended singular spectrum analysis (Ji et al., 2023). CSR RL06 mascon data are represented on 0.25° grids instead of 0.5°, which benefits the proper partition of land and ocean and is more suitable for the mass change estimation of the small-scale mountain glaciers. In the mascon solutions, all C_{20} (degree 2 order 0) coefficients were replaced with the corresponding solutions from satellite laser ranging (Loomis et al., 2020), and the C_{30} (degree 3 order 0) coefficients were replaced only for the GRACE-FO period to improve the accuracy of AIS mass change estimates. The degree-1 coefficients (geo-centre) were added back with those provided in TN-13a (Swenson et al., 2008; Sun et al., 2016; Landerer, 2019). The glacial isostatic

adjustment (GIA) was applied based on the ICE6G-D model (Peltier et al., 2018). Here, we perform the LIA correction with the data and a method similar to Wouters et al. (2019), and the results of the LIA correction for individual glaciers are shown in Table 2. The hydrological correction is carried out with 0.25 °×0.25° gridded GLDAS (Global Land Data Assimilation System) NOAH model (Rodell et al., 2016), which simulates the hydrologic signals for global land excluding the GrIS and AIS. In this study, the mass change is derived with the mean of the study period removed, and thereby, the estimated mass changes are relative to the study period. The RGI glacier 0.25 °×0.25°grid mask data are used to retrieve the mass changes of the 17 RGI regions considered in this study. In addition, the boundary data from Zwally et al. (2012) are used for the AIS and GrIS mass change estimates. Then, the time series of mass changes for individual glaciers is derived by summing the values with the glacier covered. The associated mass change contribution to GMSL rise is determined using the relationship that 360 Gt of mass variation corresponds to 1 mm of global mean sea level (GMSL) change (Rignot et al., 2019).

2.3 Mass change trend estimation and its uncertainty

The long-term mass change trend is determined by least squares fitting to the mass anomaly time series, with the model containing bias, trend, and annual and semi-annual terms, as depicted in Equation (1),

$$M(t) = at + b + A_1 \cos\left(\frac{2\pi}{T_1}t - \theta_1\right) + A_2 \cos\left(\frac{2\pi}{T_2}t - \theta_2\right) \quad (1)$$

where t is the epoch with the unit of year, $M(t)$ is the corresponding mass variation for a region (or a grid point), a denotes the linear trend, b is the offset (or bias), A_1 and A_2 represent the annual and semi-annual amplitudes and θ_1 and θ_2 are the corresponding phases. The biennial mass change trend is also calculated with this fitting model, starting in January of the first year and ending in December of the second year. The interannual mass anomaly is derived by removing the terms of linear trend. The uncertainty of the estimated mass change trend is derived from the law of error propagation according to the fitting error, GIA error, and LIA error.

2.4 Climate indices

To investigate the driving factors of global ice mass changes, we consider 11 climate indices in this study: PDO (Pacific Decadal Oscillation), MEI (Multivariate ENSO Index), NPGO (North Pacific Gyre Oscillation), AMO (Atlantic Multidecadal Oscillation), NAO (North Atlantic Oscillation), DMI (Dipole Mode Index), AO (Arctic Oscillation), SAM (Southern Annular Mode), NPI (North Pacific Index), QBO (Quasi-Biennial Oscillation) and SOI (Southern Oscillation Index). The PDO is characterized by a basin-wide dipole pattern, and it divides the North Pacific into distinctive regions following a recognizable northeast-southwest chevron pattern. Both the MEI and SOI are commonly employed for diagnosing the ENSO (El Niño and Southern Oscillation) phenomenon. The NPGO reveals a dual-gyre pattern in the North Pacific and a multidecadal oscillation of sea surface temperatures (SST) across the entire Atlantic basin. The NAO significantly influences the intensity and positioning of the North Atlantic jet streams and storm tracks and regulates heat and moisture transport. Tightly linked with ENSO, the IOD (Indian Ocean Dipole) comprises an interannual SST oscillation in the equatorial Indian Ocean, forming a characteristic west-east dipole pattern quantified using the DMI. The AO exhibits a strong connection with the NAO. During its positive phases, cold air masses tend to be confined to high latitudes due to robust circular winds. In contrast, during the negative phases, cold air masses can more readily move southward, heightening storm activity in mid-latitudes. The SAM, also known as the Antarctic oscillation (AAO), is the primary driver of climate variability in the Southern Hemisphere. It has been demonstrated to influence wind patterns, storm activity, rainfall, and temperatures ranging from the subtropics to Antarctica. The NP is defined to gauge interannual to decadal variations in atmospheric circulation. Finally, the QBO represents a quasi-periodic oscillation of the equatorial zonal wind in the tropical stratosphere, oscillating between easterly and westerly phases, with an average period of 28 to 29 months. Further details regarding the definitions of these climate indices can be found in Table 1.

2.5 Cross-correlation analysis

Since climate change may precede the mass variations of global ice, the time-lagged cross-correlation analysis is applied to the time series of interannual ice mass variations and the climate indices to assess the strength of their relationship. Cross-correlation is given by

$$R(\tau) = \frac{\sum_{i=1}^{n}[(x(i) - \bar{x})(y(i+\tau) - \bar{y})]}{\sqrt{\sum_{i=1}^{n}(x(i) - \bar{x})^2}\sqrt{\sum_{i=1}^{n}(y(i) - \bar{y})^2}} \quad (2)$$

where x and y are the time series under consideration, $\bar{x}$ and $\bar{y}$ are the corresponding means, and n is the epoch of the time series and τ is the lagged time, with a threshold of 12 months in this study. The dominant driving factor and corresponding lagging time are determined based on the maximum correlation of the two series.

Table 1. Definition of 11 used climate indices (Pfefer et al., 2022)

climate index	definition
PDO	leading EOF of SST anomalies north of 20° N in the Pacific region
MEI	the leading component of the combined EOF analysis of sea level pressure (SLP), sea surface temperature (SST), zonal and meridional components of the surface wind, and outgoing longwave radiation (OLR) over the tropical Pacific basin (30° S–30° N and 100° E–70° W)
NPGO	the second mode of sea surface height variability in the Northeast Pacific (180° W–110° W; 25° N–62° N).
AMO	it consists of a multidecadal SST oscillation across the whole Atlantic basin, with cool and warm phases that may last for 20–40 years
NAO	the first mode of a Rotated Principal Component Analysis (RPCA) applied on monthly mean 500 millibar height anomaly data from 1950 to 2000 over 0–90° N of latitude
DMI	the difference of SST averaged in the western (50° E–70° E and 10° S–10° N) and eastern (90° E–110° E and 10° S–0° N) equatorial Indian Ocean
AO	the leading EOF mode of monthly mean 1000 millibar height anomaly data from 1979 to 2000 over 20° N–90° N.
SAM	zonal pressure difference between the latitudes of 40° S and 65° S reflects the contraction (in a positive phase) or expansion (in a negative phase) of the westerly winds belt circling Antarctica.
NPI	the area-weighted sea level pressure over the region 30°N–65°N, 160°E–140°W.
QBO	quasi-periodic oscillation of the equatorial zonal wind between easterlies and westerlies in the tropical stratosphere with a mean period of 28 to 29 months.
SOI	a standardized index based on the observed sea level pressure differences between Tahiti and Darwin, Australia.

3. RESULTS AND DISCUSSION

3.1 Mass changes of ice sheets and global mountain glaciers

To comprehensively analyze the temporal characteristics of global land ice mass changes and their contributions to GMSL, we present the time series of ice mass changes for the sum of 17 mountain glaciers, the GrIS, the AIS, and their total in Figure 2 (a). Correspondingly, Figure 2 (b) illustrates the biennial trends in mass changes. From April 2002 to December 2022, all three components, including global mountain glaciers, the GrIS, and the AIS, exhibited evident mass loss trends, accompanied by annual and interannual variations. There is a total mass loss of 13,951 Gt, with individual contributions of 5,033 Gt, 4,605 Gt, and 4,313 Gt from global mountain glaciers, the GrIS and AIS, respectively. Consequently, the GMSL contributions were 13.98 mm, 12.80 mm, and 11.98 mm. The average mass change trends were –224.90±32.02 Gt/yr, –266.80±7.37 Gt/yr, and –143.64±8.86 Gt/yr, respectively. The biennial mass change trends exhibited strong interannual variations. With the smallest mass change trend observed in the AIS, it even exhibited positive mass change trends in 2005-2006, 2011-2012, 2015-2016, and 2021-2022, counterbalancing the contributions of other ice components to sea-level change. Out of the 10 biennial periods studied, there are six periods for which the mass change in all global mountain glaciers exceeded that of the GrIS; in 2019–2020, the contribution from global mountain glaciers even exceeded the sum of both ice sheets, indicating the importance of glaciers mass loss for the recent two decades.

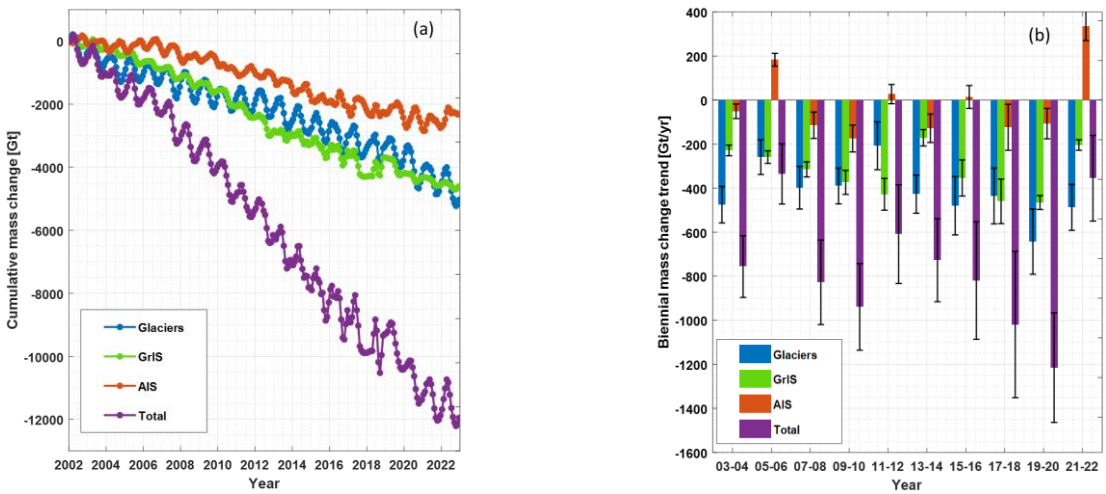

Figure 2. Mass changes over global ice sheets and glaciers from April 2002 and December 2022 (a): Cumulative mass changes of global mountain glaciers, the GrIS and AIS, are shown in gigatonnes [Gt]; (b) corresponding biennial mass change trends are shown in Gt per year [Gt/yr].

3.2 Mass changes in 17 global mountain glaciers

The mass change time series and biennial mass change trends for 17 mountain glaciers are shown in Figure 3. Overall, Alaska exhibits the most significant glacier melting trend at –72.38±4.76 Gt/yr, corresponding to a GMSL contribution of 0.20±0.013 mm/yr. Additionally, the Arctic Canada North, Arctic Canada South, High Mountain Asia, and Southern Andes glaciers show apparent melting trends exceeding 20 Gt/yr. The results suggested the importance of focusing future scientific investigations of ice mass change on Alaska, Arctic Canada, High Mountain Asia, and the Southern Andes (primarily the Patagonia).

Table 2. Linear trend of ice mass change from April 2002 to December 2022

RGI number	Region name	LIA [Gt/yr]	GIA (Gt/yr)	Mass change (Gt/yr)*	GMSL (mm/yr)
01	Alaska	7±4	–0.84±1.91	–72.38±4.76	0.20±0.013
02	Western Canada & USA	0±0	0.05±4.22	–4.96±4.41	0.01±0.012
03	Arctic Canada North	0±0	5.82±0.34	–36.05±0.99	0.10±0.003
04	Arctic Canada South	0±0	13.52±1.22	–27.19±1.39	0.08±0.004
06	Iceland	3±2	–1.29±0.28	–11.14±1.59	0.03±0.004
07	Svalbard and Jan Mayen	0±0	2.03±0.10	–17.78±0.92	0.05±0.003
08	Scandinavia	0±0	16.18±0.63	3.46±0.86	0.01±0.002
09	Russian Arctic	0±0	6.32±0.11	–17.77±0.98	0.05±0.003
10	North Asia	0±0	2.44±0.88	3.46±1.06	–0.01±0.003
11	Central Europe	0±0	–1.80±2.19	–4.90±2.33	0.01±0.007
12	Caucasus and Middle East	0±0	0.09±0.06	–1.49±0.16	0.004±0.0001
13–15	High Mountain Asia	3±1	11.45±4.22	–23.00±4.60	0.06±0.013
16	Low Latitudes	0±0	1.41±1.62	6.86±1.87	–0.02±0.005
17	Southern Andes	9±5	17.09±1.60	–24.27±5.54	0.07±0.015
18	New Zealand	0±0	–1.05±0.16	3.53±0.57	–0.01±0.002
–	Global MGs	22±7	71.41±19.55	–224.90±32.02	0.63±0.089
05	Greenland Ice Sheet	–	1.50±6.48	–266.80±7.37	0.68±0.021
19	Antarctic Ice Sheet	–	87.58±7.86	–143.64±8.86	0.40±0.025
–	Global total	–	160.50±33.89	–613.24±41.73	1.64±0.120

*Note that the mass change error is derived by the error propagation from GIA error and fitting error. Regional glacier areas are from RGI 6.0 and refer to the first decade of the twenty-first century (RGI Consortium Randolph Glacier Inventory, 2017).

Figure 3 displays the time series of glacier mass changes and the biennial mass change trends for each RGI glacier region. In general, glacier ice mass changes show a significant loss trend, except for Scandinavia, North Asia, low latitudes, and New Zealand, which exhibit a slight mass gain trend. The biennial mass change trends (the bar charts in Figure 3) show distinct interannual variations across all glaciers. Specifically, the Alaska glacier exhibited the most substantial mass loss trend at –243.2 ± 39.02 Gt/yr between 2009 and 2010; in contrast, the mass change trend was relatively weak during 2011–2012, with the glacier mass remaining relatively stable. Western Canada and USA glaciers showed relatively modest mass change trends but displayed strong annual and interannual variations. Arctic Canada North experienced its strongest mass loss trend during 2011–2012 and remained relatively stable during 2013-2014. For Arctic Canada South, negative mass change trends persisted throughout these ten biennial periods, ranging from –17.98 to –73.07 Gt/yr. Due to their smaller ice coverage, Icelandic glaciers exhibited relatively weaker mass loss trends but consistently contributed to sea-level rise, especially during 2003–2004, 2017–2018, and 2021–2022.

SJM glaciers showed a noticeable melting trend during 2003-2004, remained stable during 2005–2010, and sustained a loss of 343 Gt of ice mass from 2011 to 2022, roughly equivalent to 0.95 mm of global mean sea-level rise. Scandinavia and North Asia glaciers exhibited long-term mass growth trends of 3.46±0.86 Gt/yr, but short-term mass loss may be evident in their biennial mass change trends. Among the three glaciers in the Southern Hemisphere, particularly the Patagonia Glacier in the Southern Andes, they have positively contributed to sea-level change.

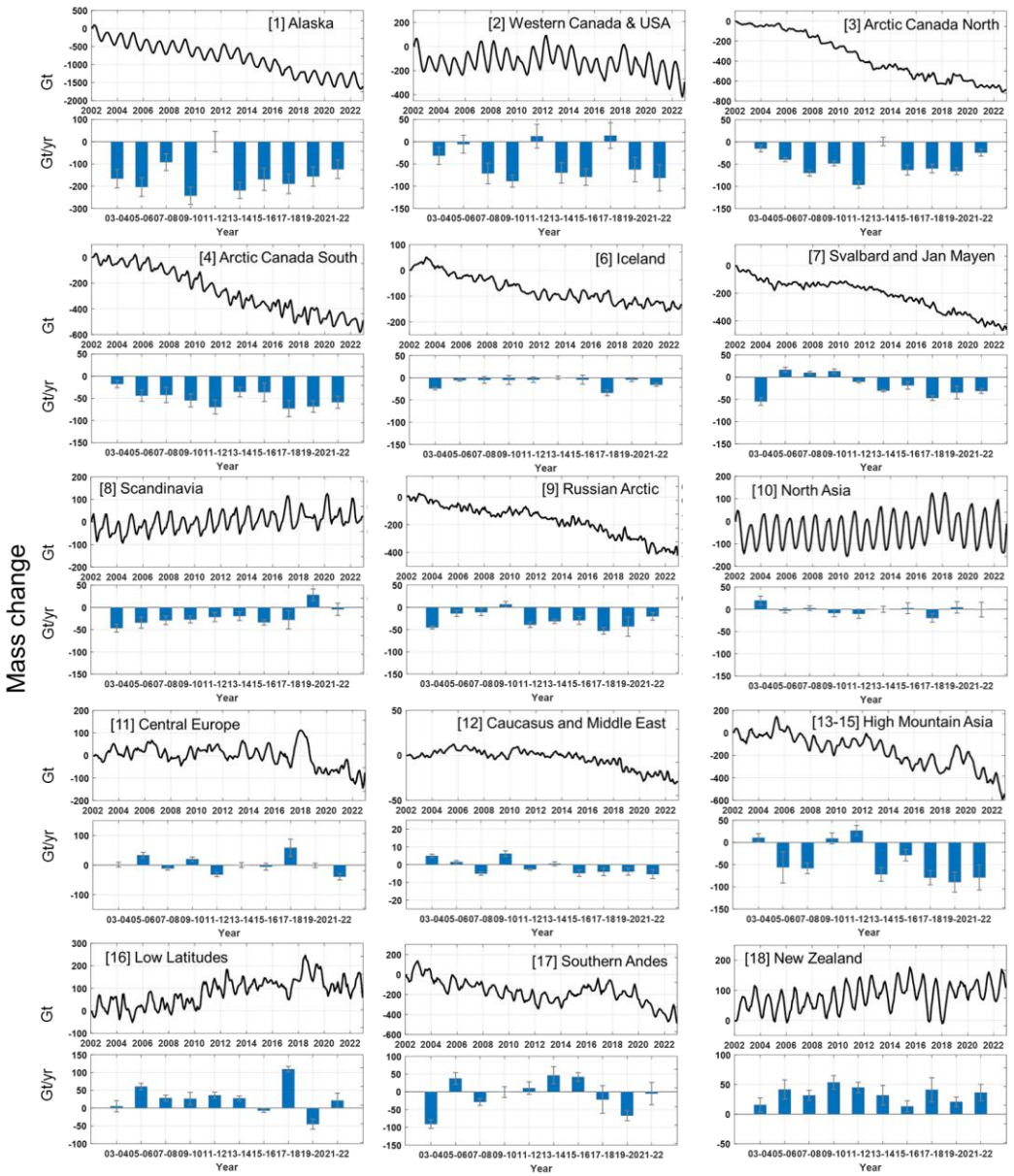

Figure 3. Time series of glacier mass changes for each RGI glacier region. The black line (upper sub-figure) displays the cumulative mass change in Gt. The bars (lower sub-figure) display biennial mass change trends in gigatonnes per year [Gt/yr] with error bars.

The spatial patterns of global ice mass change trends are shown in Figure 4. Over the GrIS, significant mass loss is found in the coastal margins, and there are evident mass gain signals over the inner region. As for the AIS, pronounced mass loss trends are found in the Antarctic Peninsula, coastal west AIS, and Totten glaciers of the east AIS, with mass gains in the Kamb stream and DML. Additionally, the Arctic glaciers of RGI3, RGI4, RGI6, RGI7, and RGI9, Alaska, and Patagonia glaciers show an apparent mass loss trend.

3.3 Comparison with other mass change estimates

We compared our mass change trends of global mountain glaciers with those from the previous studies and depicted the results in Figure 5. It is shown that our result is the latest, updated to December 2022. It exhibits excellent consistency within the uncertainty range with previous findings, excluding that of Jacob et al. (2012), indicating that the improved GRACE/GRACE-FO mascon solutions are beneficial for estimating mountain glacier mass changes. The estimate in Jacob et al. (2012) appears to be lower than others, which could be primarily attributed to their earlier study period of 2003–2010, highlighting the differences in results generated during that timeframe. This also implies that the trend in glacier melting has intensified over the past decade, consistent with the estimates shown in Figure 2 (b).

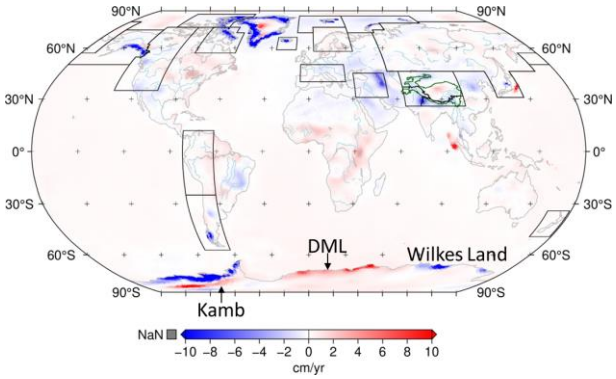

Figure 4. The spatial patterns of a linear trend in ice mass changes derived from CSR mascon solutions. DML is short for the Dronning Maud Land.

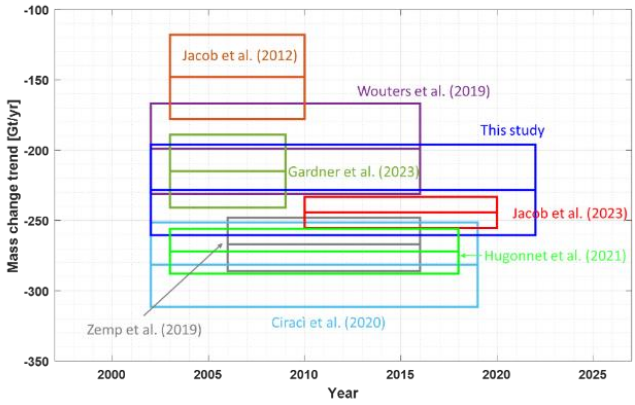

Figure 5. Various published global estimates of global mass change and their respective time spans with uncertainties.

To further compare the estimates from the CSR mascon with previous estimations, we compare the glacier-scale ice mass change trend estimates to those from the observations of in-situ measurements (i.e., Zemp et al. (2019)), ASTER (i.e., Hugonnet et al. (2021)), and Crysat2 satellite altimetry data (i.e., Jacob et al. (2023)). The study periods are trucked for 2006–2016, 2000–2019, and 2010–2020, respectively. Results are presented in scatter plots in Figure 6 (a–c), where the horizontal axis represents the CSR mascon estimate, and the vertical axis corresponds to the trend estimates from Zemp et al. (2019), Hugonnet et al. (2021), and Jacob et al. (2023). Then, we computed the linear regression coefficient (ranging from –1 to +1), intercept and Pearson's correlation coefficient (r, ranging from –1 to +1) by using linear regression fitting to evaluate the consistency of the CSR mascon estimates with those from the three mentioned literature. The fitting results are also depicted in Figure 6(a–c). The CSR mascon estimates align pretty well with the estimates from Zemp et al. (2019) and Hugonnet et al. (2021), although the in-situ measurements show a high uncertainty of up to 84 Gt/yr in Arctic Canada North. In contrast, the CSR mascon estimates show a closer alignment with the results of Hugonnet et al. (2021), with a slope of 0.9±0.1 and an intercept of –1.2±3.0. At the glacier scale, the estimates from Jacob et al. (2023) exhibit the most noticeable differences when compared to CSR mascon. However, there is overall good agreement (Figure 5), indicating that further study should be carried out to improve the accuracy of the ice mass change estimates from Crysat2 satellite altimetry data.

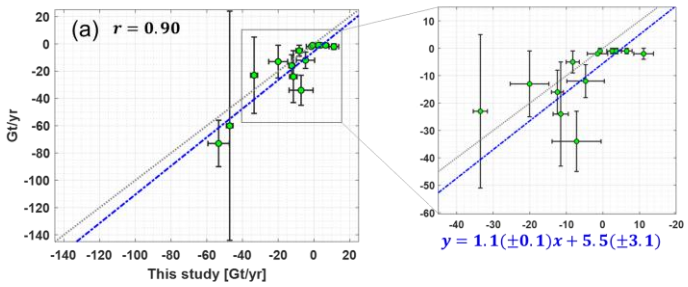

Figure 6. Mass change trends of mass change in global mountain glaciers with given uncertainties. (a): Zemp et al. (2019), (b): Hugonnet et al. (2021), and (c): Jacob et al. (2023).

3.4 Links to atmospheric circulation

Figure 7 illustrates the time-lagged correlation coefficients between interannual mass variations and climate indices. This analysis aims to explore the primary influencing factors and the corresponding time delays. Concerning climate-related factors, NPGO, PDO, MEI, and SOI emerge as the predominant drivers of global glacier and ice sheet mass fluctuations, showing stronger correlations. Specifically, NPGO plays a significant role in modulating the interannual variations in ice mass for regions including Alaska, Arctic Canada, Svalbard, Jan Mayen, the Russian Arctic, the Caucasus, the Middle East, and the GrIS. It is the most crucial climate index for predicting ice mass fluctuations.

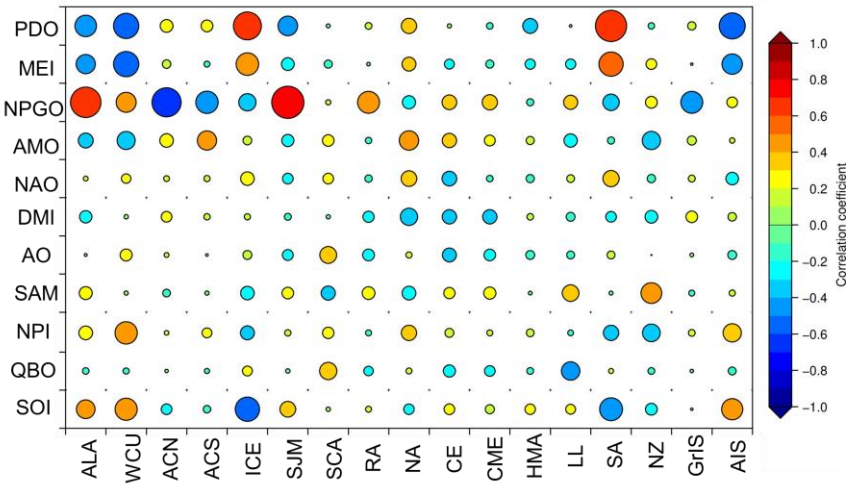

Figure 7. Correlation coefficients between interannual mass variations and climate indices for 17 mountain glaciers and polar ice sheets.

Table 3. Dominant climatic driving factors of ice mass change and the lag times.

RGI number	Region name	Climate index	correlation coefficients	lagged times [month]
01	Alaska	NPGO	0.67	12
02	Western Canada & USA	MEI	–0.55	8
03	Arctic Canada North	NPGO	–0.64	6
04	Arctic Canada South	NPGO	–0.49	6
06	Iceland	PDO	0.61	7
07	Svalbard and Jan Mayen	NPGO	0.70	0
08	Scandinavia	QBO	0.38	12
09	Russian Arctic	NPGO	0.48	12
10	North Asia	AMO	0.42	8
11	Central Europe	NAO	–0.32	11
12	Caucasus and Middle East	NPGO	0.34	12
13–15	High Mountain Asia	PDO	–0.33	0
16	Low Latitudes	QBO	–0.40	11
17	Southern Andes	PDO	0.68	3
18	New Zealand	SAM	0.45	0
05	Greenland Ice Sheet	NPGO	–0.48	7
19	Antarctic Ice Sheet	PDO	–0.57	10

4. CONCLUSIONS

Using the latest CSR mascon data, we conducted a comprehensive study on global land ice, encompassing 17 mountain glaciers, the Greenland Ice Sheet, and the Antarctic Ice Sheet from April 2002 to December 2022. We analyzed their mass changes and assessed their contributions to GMSL while uncovering the driving forces behind their interannual mass variations. Overall, the cumulative ice mass loss amounts to 13,951 Gt per year, translating to a GMSL rise of 1.6 ± 0.1 mm per year. Specifically, the contributions from global MGs, the Greenland Ice Sheet GrIS, and the AIS are approximate –224.90 ± 32.02 Gt per year, –266.80 ± 7.37 Gt per year, and –143.64 ± 8.86 Gt per year, respectively. Significantly, among the 17 MGs examined, the Alaska glacier exhibits the most substantial loss trend at –72.38 ± 4.76 Gt per year, constituting approximately one-third of the total MG mass loss. Following closely are the Arctic Canada North, Arctic Canada South, Southern Andes, and High Mountain Asia glaciers, with mass loss trends of –36.05 ± 0.99, –27.19 ± 1.39, –24.27 ± 5.54, and –23.00 ± 4.60 Gt per year, respectively. When analyzing biennial mass changes, we observe significant interannual variations for individual glaciers, closely linked to anomalies in atmospheric circulation. Among the 11 climate indices considered, the NPGO, PDO, and MEI emerge as the most pivotal climate indices for predicting variations in ice mass and subsequent sea-level fluctuations.

5. ACKNOWLEDGEMENTS

This work is sponsored by the Natural Science Foundation of China [grant numbers: 42274005, 41974002, 42061134010]. Ph.D. student Kunpu Ji is acknowledged for filling the data gap between GRACE and GRACE-FO mission.

6. REFERENCES

Arendt, A., Luthcke, S., Gardner, A. et al. 2013. Analysis of a GRACE global mascon solution for Gulf of Alaska glaciers. *Journal of Glaciology*, 59(217), pp. 913–924.

Ciracì, E., Velicogna, I., & Sutterley, T. 2018. Mass Balance of Novaya Zemlya Archipelago, Russian High Arctic, Using Time-Variable Gravity from GRACE and Altimetry Data from ICESat and CryoSat-2. *Remote Sensing*, 10, 1817.

Ciracì, E., Velicogna, I., & Swenson, S. 2020. Continuity of the mass loss of the world's glaciers and ice caps from the GRACE and GRACE Follow-On missions. *Geophysical Research Letters*, 47, e2019GL086926.

Doumbia, C., Castellazzi, P., Rousseau, A. N., et al. 2019. High Resolution Mapping of Ice Mass Loss in the Gulf of Alaska From Constrained Forward Modeling of GRACE Data. *Front. Earth Sci.*, 7, 360.

Farinotti D., Huss M., Fürst J., et al. 2019. A consensus estimate for the ice thickness distribution of all glaciers on Earth. *Nature Geoscience*, 12, pp. 168–173.

Gardner, A., Moholdt, G., Wouters, B., et al. 2011. Sharply increased mass loss from glaciers and ice caps in the Canadian Arctic Archipelago. *Nature*, 473, pp. 357–360

Gardner, A., Moholdt, G., Cogley, J., et al. 2013. A Reconciled Estimate of Glacier Contributions to Sea Level Rise: 2003 to 2009. *Science*, 340(6134), pp. 852-857.

Hugonnet, R., McNabb, R., Berthier, E., et al. 2021. Accelerated global glacier mass loss in the early twenty-first century. *Nature*, 592, pp. 726–731.

Landerer, F., 2019. Monthly estimates of degree-1 (geocenter) gravity coefficients,generated from GRACE (04-2002-06/2017) and GRACE-FO (06/2018 onwardRL06 solutions. In: GRACE Technical Note 13, The GRACE Project. NASA JetPropulsion Laboratory.

Jacob, T., Wahr, J., Pfeffer, W. T., et al. 2012. Recent contributions of glaciers and ice caps to sea level rise. *Nature*, 482, PP. 514–518.

Jacob, L., & Gourmelen, N. 2023. Glacier mass loss between 2010 and 2020 dominated by atmospheric forcing. *Geophysical Research Letters*, 50, e2023GL102954. https://doi.org/10.1029/2023GL102954.

Ji, K., Shen, Y., Chen, Q, et al. 2023. Extended singular spectrum analysis for processing incomplete heterogeneous geodetic time series. *Journal of Geodesy*, 97, 74.

Loomis, B. D., Rachlin, K. E., Wiese, D. N., Landerer, F. W., & Luthcke, S. B. 2020. Replacing GRACE/GRACE-FO C30 with satellite laser ranging: Impacts on Antarctic Ice Sheet mass change. *Geophysical Research Letters*, 47, e2019GL085488.

Lythe, M.B., Vaughan, D.G., and the BEDMAP Consortium. 2001. BEDMAP: a new ice thickness and subglacial topographical model of Antarctica. *Journal of Geophysical Research*, 106(B6), pp. 11335–11351.

Morlighem, M. et al. 2017. BedMachine v3: complete bed topography and ocean bathymetry mapping of Greenland from multibeam echo sounding combined with mass conservation. *Geophys. Res. Lett.,* 44, pp. 11,051–11,061.

Peltier, W. R., Argus, D. F., & Drummond, R. (2018). Comment on "An Assessment of the ICE-6G_C (VM5a) Glacial Isostatic Adjustment Model" by Purcell et al. J. Geophys. Res. Solid Earth, 123(2), pp. 2019–2028.

Pfefer, J., Cazenave, A., & Barnoud, A. 2022. Analysis of the interannual variability in satellite gravity solutions: detection of climate modes fngerprints in water mass displacements across continents and oceans *Climate Dynamics*, 58, 1065–1084.

RGI Consortium Randolph Glacier Inventory (v.6.0): A Dataset of Global Glacier Outlines. Global Land Ice Measurements from Space, Boulder, Colorado USA (RGI Technical Report, 2017). https://doi.org/10.7265/N5-RGI-60.

Rodell, M., & Beaudoing, H. (2016). GLDAS Noah Land Surface Model L4 3 hourly 0.25 × 0.25 degree V2.1. https://doi.org/10.5067/E7TYRXPJKWOQ

Rignot, E., Mouginot, J., Scheuchl, B., Van den Broeke, M., van Wessem, M. J., and Morlighem, M. 2019. Four Decades of Antarctic Ice Sheet Mass Balance from 1979-2017. *Proc. Natl. Acad. Sci.*, 116, 1095–1103.

Save, H., S. Bettadpur, and B.D. Tapley. 2016. High resolution CSR GRACE RL05 mascons, *J. Geophys. Res. Solid Earth*, 121, doi:10.1002/2016JB013007.

Save, Himanshu, 2020, "CSR GRACE and GRACE-FO RL06 Mascon Solutions v02", doi: 10.15781/cgq9-nh24.

Schneider, D. P., C. Deser, J. Fasullo, and K. E. Trenberth, 2013: Climate Data Guide Spurs Discovery and Understanding. Eos Trans. *AGU*, 94, 121–122, https://doi.org/10.1002/2013eo130001

Swenson, S., D. Chambers, and J. Wahr. 2008. Estimating geo-center variations from a combination of GRACE and ocean model output, Journal of Geophysical Research: Solid Earth, 113(8), B08410. doi:10.1029/2007JB005338.

Sun, Y., R. Riva, and P. Ditmar. 2016, Optimizing estimates of annual variations and trends in geocenter motion and J2 from a combination of GRACE data and geophysical models, Journal of Geophysical Research: Solid Earth, 121.

WGMS (2021): Global Glacier Change Bulletin No. 4 (2018-2019). Zemp, M., Nussbaumer, S. U., Gärtner-Roer, I., Bannwart, J., Paul, F., and Hoelzle, M. (eds.), ISC(WDS)/IUGG(IACS)/ UNEP/UNESCO/WMO, World Glacier Monitoring Service, Zurich, Switzerland, 278 pp.

Wouters, B., Gardner, A., & Moholdt, G. 2019. Global Glacier Mass Loss During the GRACE Satellite Mission (2002-2016). *Front. Earth Sci*., 7(96). doi: 10.3389/feart.2019.00096

Xiang, L., Wang, H., Jiang, L. et al. 2021. Glacier mass balance in High Mountain Asia inferred from a GRACE release-6 gravity solution for the period 2002–2016. *J. Arid Land*, 13(3), pp. 224–238.

Zwally, H. J. et al. 2002. ICESat's lasermeasurements of polar ice, atmosphere, ocean, and land. J. Geodyn. 34, pp. 405–445.

Zwally, H.; Giovinetto, M.; Beckley, M.; Saba, J. (2012). Antarctic and Greenland Drainage Systems. Available online: http://icesat4.gsfc.nasa.gov/cryo_data/ant_grn_drainage_systems.php